

tion across modalities, facilitating collaborative knowledge acquisition from large-scale data. To mitigate potential semantic information loss when elevating images to BEV, we introduce a Masked Autoencoder (MAE) loss for the image modality, ensuring precise semantic capture. Our approach is designed to train backbones of both image and point cloud modalities from scratch, making it well-suited for investigating the effects of large-scale data pre-training on multi-modal 3D perception models.

Secondly, we address the domain gap between datasets. 3D data for autonomous driving are typically collected independently using specialized equipment in different road environments, resulting in varied datasets. These datasets may come from different public sources or be privately collected by companies and organizations at various locations, times, and using different equipment. As a result, data from different sources may exhibit significant distributional differences. The distributional bias may lead to training conflicts, resulting in suboptimal outcomes when they are combined for model training. This hinders the further expansion of the training data scale for 3D perception models.

To mitigate the impact of domain gap between datasets, we employ a prompt adapter-based training strategy [67] to disentangle dataset biases from the backbone network. We set learnable prompt parameters for different datasets, which are activated separately during the training process and connected to the backbone network via an adapter. This method allows the model to leverage larger and more diverse data sources more effectively.

In this paper, we propose a self-supervised pre-training framework which can leverage heterogeneous unlabeled datasets for 3D perception models in autonomous driving. Our framework is designed to reduce dependency on large annotated datasets and enhance the data scalability in 3D perception domain. The results in four downstream tasks, 3D object detection, 3D object tracking, BEV segmentation, and occupancy prediction demonstrate that our method can effectively improve model performance with heterogeneous unlabeled datasets. Meanwhile, through our pre-training method, the performance of 3D perception models shows a steady improvement as the amount of training data increases, demonstrating the potential to expand the frontier of 3D perception models.

To summarize, we make the following contributions:

- We propose a self-supervised pre-training method which is able to learn effective 3D representations from scratch on a combination of heterogeneous datasets.
- We evaluate our model on four tasks: 3D object detection, 3D object tracking, BEV segmentation and occupancy prediction, and demonstrate the effectiveness of our method.
- We scale up the training data volume to 250,000 frames. We observe that the models demonstrate steady perfor-

mance improvement as the training data volume scales up, which suggests that our method can be further scaled with additional training resources.

2. Preliminary

In this section, we present the idea of self-supervised pre-training and categorize the proposed approaches for 3D perception into two groups.

Self-supervised pre-training Self-supervised pre-training is a method in which models are trained by constructing pretext tasks, with training labels derived from the data itself. This allows models to learn preliminary knowledge from unlabeled data and converge more efficiently on downstream tasks. In the field of 3D perception, this method is commonly employed to train backbone encoders [83], enabling them to acquire accurate and effective feature encoding capabilities, which can be utilized in subsequent downstream tasks.

In recent studies on 3D perception, the pretext tasks for self-supervised pre-training are typically divided into two categories: contrastive learning and masked autoencoders. We will introduce both approaches in detail below.

Contrastive learning Contrastive learning aims to learn representations by contrasting positive and negative data pairs. This can be applied to representation learning within a single modality [16, 70] or to align different modalities [45, 51]. When applied to a single modality, different views of the same data frame are typically treated as positive samples, while different frames serve as negative samples. This approach helps the model to learn semantic information by supervising it to accurately differentiate data frames. In the case of aligning different modalities, matching pairs of data from the dataset (e.g., point clouds and images at the same moment) are considered positive samples, while non-matching pairs are treated as negative samples, allowing the model to learn similar semantic representations across modalities.

Masked-autoencoder The Masked-Autoencoder (MAE) method [17] involves masking a portion of the input image or point cloud, after which the encoder model encodes the remaining visible parts into a feature sequence. An additional decoder module is then used to reconstruct the masked portion. The MAE approach helps the model learn semantic information and local features embedded in the image or point cloud by making it predict the masked regions based on the unmasked parts. This enables the network to extract meaningful features, improving perception accuracy on downstream tasks.

3. Method

3.1. Design of training losses

To effectively utilize unlabeled data, we design two kinds of losses in our framework. Firstly, we perform contrastive learning on the BEV features of both image and point cloud modalities. This process allows the unique features within each modality to mutually inspire and guide the model toward learning more effective feature representations. Secondly, as images are collected as a 2D space, there is a risk of losing semantic information during the process of elevating it to 3D and transforming it into BEV. We then apply a self-supervised loss to maintain their semantic information. Previous research [42] has pointed out that MAE, compared to contrastive learning-based methods performs better in scenarios involving complex decoder fine-tuning, which aligns with our use case. We therefore use MAE loss as the self-supervised loss within image modality.

As shown in figure 1, our overall training loss is the combination of the two losses, which can be expressed as:

$$\begin{aligned} \mathcal{L}_{\text{All}}(\theta; D) = & \mathcal{L}_{\text{MAE}}(\theta_{\text{img}}; D_{\text{img}}) \\ & + \mathcal{L}_{\text{CL}}(\theta_{\text{img}}, \theta_{\text{pcd}}; D_{\text{img}}, D_{\text{pcd}}) \end{aligned} \quad (1)$$

where θ represents the model’s parameters and D refers to the model’s inputs. D_{img} and D_{pcd} refers to input data of images and point clouds, respectively. While θ_{img} and θ_{pcd} refers to the parameters of sub-network which process D_{img} and D_{pcd} . We then introduce the two training losses within our framework in detail:

Contrastive loss Each sample D_i from dataset \mathcal{D} consists of paired image and point cloud data, $D_i = \{I_i, P_i\}$. After serialization, the data from both modalities are fed into their respective backbone networks, f_{img} for the image and f_{pcd} for the point cloud. The point cloud features can be directly transformed into the BEV (Bird’s Eye View) perspective, while the image features are projected into the BEV space using the LSS (Lift, Splat, Shoot) network, leveraging the camera extrinsic parameters θ_{ce} , i.e.

$$\begin{aligned} BEV_{\text{img}} &= LSS(f_{\text{img}}(I_i), \theta_{ce}) \\ BEV_{\text{pcd}} &= f_{\text{pcd}}(P_i) \end{aligned} \quad (2)$$

The BEV maps are formed with 128×128 grids and we take the grids in corresponding positions $m \in [0, 128 \times 128)$ in image BEV maps $BEV_{\text{img}} = \{x_i^j\}$ and point cloud BEV maps $BEV_{\text{pcd}} = \{y_i^j\}$ as positive pairs (x_i^m, y_i^m) . Grids in positions not corresponding to each other are treated as negative pairs $(x_i^m, y_i^n), n \neq m$. In the actual training process, due to memory constraints, we randomly sampled some locations from the BEV map for training. We then use NCE

loss to train the model and the loss is formulated as:

$$\mathcal{L}_{\text{CL}} = - \sum_{i=1}^{|\mathcal{D}|} \frac{1}{|\mathcal{D}|} \sum_{j=1}^K \frac{1}{K} \log \frac{\exp(x_i^j \cdot y_i^j / \tau)}{\sum_{k=1}^K \exp(x_i^j \cdot y_i^k / \tau)} \quad (3)$$

where τ is temperature parameter, and K is the number of grids sampled from BEV maps for contrastive learning.

MAE loss Each of the input images I_i from dataset \mathcal{D} is divided into patches $c_i = \{c_i^j\}$, and we randomly sample a portion of the patches to be masked (i.e. set to zero). After that, all patches including the masked and unmasked ones will be passed through the SwinTransformer encoder to embed them into image tokens. After that, an additional MAE decoder processes these tokens, reconstructing the original images. The reconstruction quality is assessed using the MAE loss, guiding the network to learn meaningful image features in a self-supervised manner:

$$\mathcal{L}_{\text{MAE}} = \frac{1}{|\mathcal{D}|} \sum_{i=1}^{|\mathcal{D}|} \|\hat{c}_i - c_i\|_2^2, \quad (4)$$

where \hat{c}_i is the reconstructed image patches, and c_i is the original image patches.

3.2. Dataset prompt formulation

As discussed in section 1, naively mixing multiple 3D perception datasets for model training may lead to suboptimal performance because of the domain gap between different datasets. Therefore, we employed a Prompt Adapter design, inserting additional learnable parameters related to specific datasets into the backbone networks of both image and point cloud modalities to retain the common knowledge of different datasets within the backbone model while separating the differential information between datasets outside it. (shown in figure 2). Specifically, during multi-dataset training, we evenly mix data from different datasets and reindex them. For each dataset \mathcal{D}_i , we define a set of learnable parameters r_i as corresponding soft prompt. During training, each data sample activates the corresponding prompt parameters for computation based on its index.

Following [67], we employ an MLP adapter network to map the prompt into weight and bias parameters. These parameters are then integrated with the layer_norm of the transformer layers in the backbone network through linear operations, thus injecting the prompt into the backbones.

Therefore, for each input sample $d_i^j \in \mathcal{D}_i$, the normalization process of the data sample in the backbones can be expressed as:

$$\begin{aligned} \alpha, \beta &= Adapter(r_i), \\ PromptNorm(d_i^j) &= \alpha \times LayerNorm(d_i^j) + \beta \end{aligned} \quad (5)$$

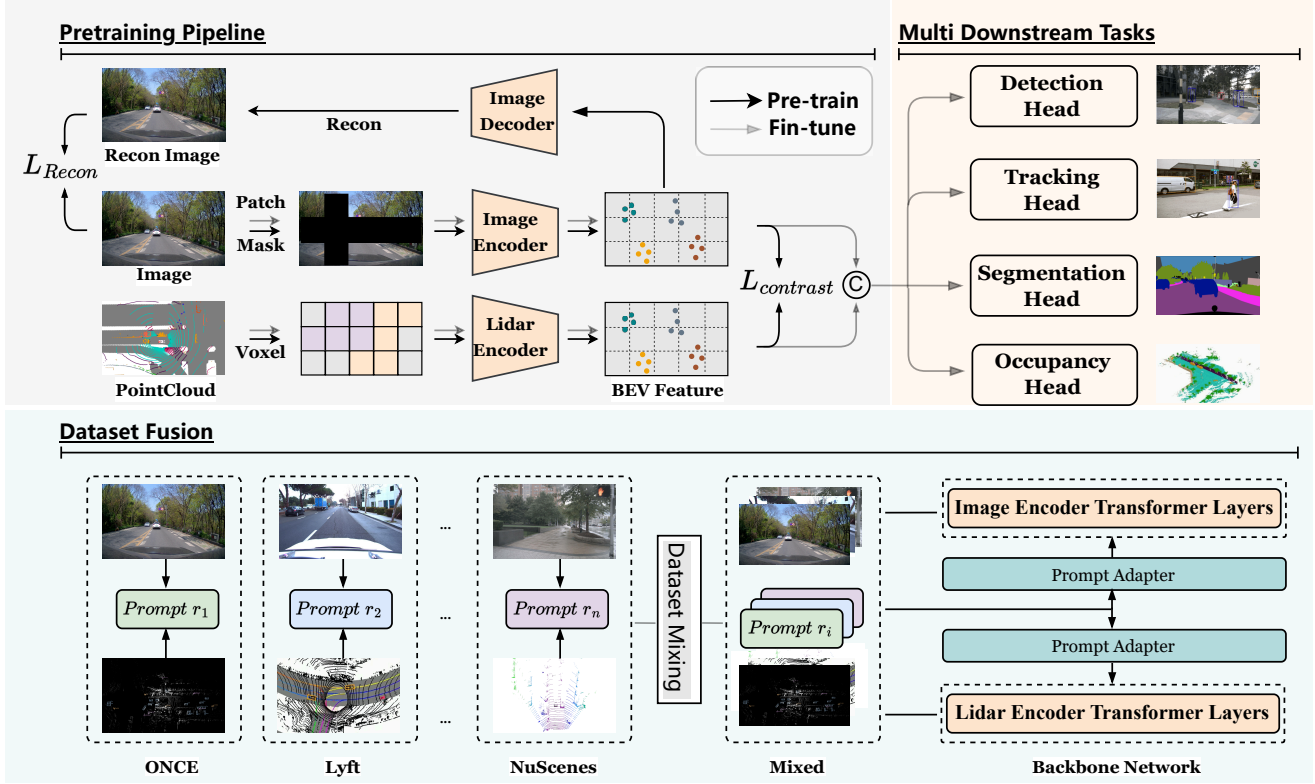


Figure 1. The pre-train-then-fine-tune framework for multi-modal 3D perception integrating image and point cloud data. The point clouds and partially masked images are encoded into BEV feature tokens. We use contrastive loss between the BEV map of the two modalities to make them co-evolve, while use mae loss of recovering the masked portion of images to help capturing their semantic features.

3.3. Optimization objective

We replace all LayerNorm layers in both the image and point cloud backbone networks with PromptNorm. Therefore, the trainable parameters during the training process include the backbone network parameters θ_b , the soft prompt $C = \{C_i\}$, and the adapter parameters θ_a .

Therefore, the final training objective becomes:

$$\operatorname{argmin}_{r, \theta_a, \theta_b} \frac{1}{N} \sum_{i=1}^N \frac{1}{|D_i|} \sum_{d_i^j \in D_i} \mathcal{L}_{All}(d_i^j; r_i; \theta_a, \theta_b) \quad (6)$$

where N is the number of datasets, θ_a is the parameters of adapters and θ_b is the parameters of backbones.

In such optimization process, the soft prompt r can be optimized for efficient representation of dataset-specific information, while the backbone network learns general knowledge and feature representations across datasets. The adapter parameters are optimized for the effective connection between the two for specific datasets.

4. Experiment & results

In this section, we first introduce the settings of our experiments. Then, we show our evaluation results of our models to demonstrate how our method leverages large-scale unlabeled data for pre-training to continually improve the performance of autonomous driving 3D perception models. We will answer following research questions (RQs):

RQ1: Can our proposed self-supervised pre-training framework effectively improve model performance on downstream tasks? (Ref. Section 4.2)

RQ2: Can the prompt adapter technique we employ help mitigating the domain gap between 3D datasets in our self-supervised pre-training framework? (Ref. Section 4.3)

RQ3: Does our proposed approach demonstrate the potential for continuous improvement in performance as the scale of data increases? (Ref. Section 4.4)

4.1. Experiment settings

Models In recent 3D perception research [14, 27, 33, 35, 57], transformer networks are gradually gaining popularity due to their stronger scalability and better performance. We adopt the Swin Transformer [32] and DSVT [57] architectures for the backbones of image and point cloud modalities,

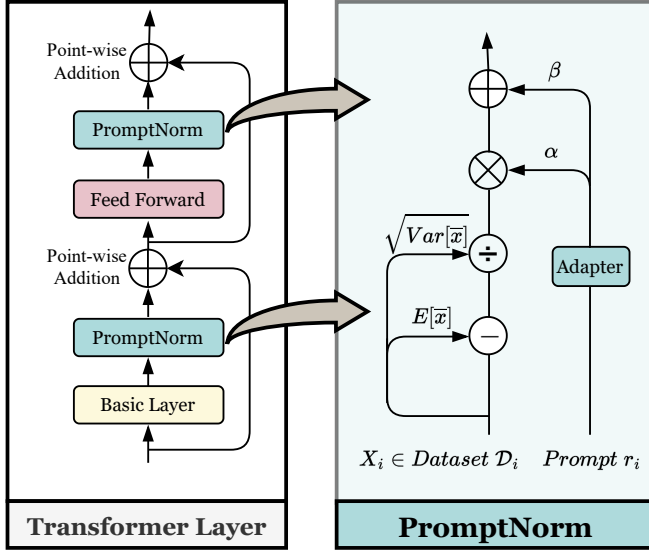


Figure 2. Multi-dataset training strategy with prompt adapters. We set tunable prompts for each dataset and mix the dataset during training. The prompts are injected into the backbones with MLP adapters.

respectively. Swin transformer is one of the most popular transformer backbones in computer vision while DSVT is one of the state-of-the-art backbones for point cloud and is also widely used in 3D perception [58, 73, 77]. For encoding image features into BEV, we employ the LSS method used in BEVFusion [28].

Datasets During the pre-training stage, we use the Nuscenes [3], Lyft [11], and ONCE [34] datasets. All of them are widely used large-scale 3D perception datasets, offering 360-degree surround-view image data and point cloud data collected by LiDARs. However, there are significant differences in their sensors: the beams for LiDAR varies, being 32, 64, and 40, respectively, and the mounting angles of the cameras also differ.

NuScenes, Lyft and ONCE, datasets provide 28,000, 22,000 and 980,000 training frames, respectively. To control the scale of the experiments, we sampled 50,000 frames from the ONCE dataset when investigating the multi-dataset training strategy. In the dataset scaling experiments, we sampled 200,000 frames from ONCE and balanced the number of training samples across datasets by repeating the data from NuScenes and Lyft four times. To align the data cross different datasets, we standardized the 6-camera surround-view visual signals and unified the LiDAR range and feature dimensions, but did not adjust the density of the points to maintain as much raw information as possible. Detailed configurations are provided in Appendix A.

For downstream benchmark, we propose two kinds of

settings. In the main setting, we use 20% of the NuScenes dataset to evaluate the model’s capabilities with a limited number of samples with annotation. This benchmark includes four downstream tasks: 3D object detection, 3D object tracking, BEV segmentation, and occupancy prediction. We also provide a held-out setting in which we use 20% portion of the Waymo Open [52] dataset as out-of-domain experimental data to validate whether our method works when the fine-tuning data distribution differs from the pre-training data. This benchmark only officially supports the 3D object detection task. Model structure and training details are provided in Appendix C.

Evaluation In 3D object detection task, we utilize official evaluation metric of NuScenes, Mean Average Precision (mAP) and nuScenes Detection Score (NDS), respectively reflecting accuracy rating and comprehensive consideration of translation, scale, angle, and velocity. For Waymo Open dataset, we utilize L1 mAP and L1 mAPH, which are also officially provided. In the 3D object tracking task, we also use the official evaluation metrics of NuScenes, Average Multi Object Tracking Accuracy (AMOTA) and Average Multi Object Tracking Precision (AMOTP), which average the MOTA and MOTP metrics at different recall thresholds. MOTA measures the accumulation of tracking errors, including false positives, missed targets, and identity switches while MOTP evaluates the misalignment between annotated and predicted bounding boxes. For BEV segmentation and occupancy prediction, we adopt mean Intersection-over-Union (mIoU) which is computed as the ratio of the intersection to the union of prediction and ground truth and averaged between classes. An overall IoU is also provided from occupancy prediction task.

4.2. Effectiveness of pre-training framework

We first evaluate the effectiveness of our pre-training framework when conducted on a single dataset. We use NuScenes dataset alone to pre-train our model and compare it with following baselines:

- Scratch: Randomly initialize the networks without any pre-training.
 - BEVDistill: State-of-the-art open-source pre-training method similar to our setting. Though it was designed to distill knowledge from pre-trained image networks, it can also be adopted to train models from scratch [9, 51].
- More discussions about baselines and related works are provided in Appendix B.

Main results & ablation study Table 1 presents a comparison of the performance on various downstream tasks between our method and baseline methods in the held-in setting. In all four tasks, our pre-training framework achieves significant performance improvements and outperforms the

Table 1. Evaluation of our pre-training framework with baseline methods on downstream tasks. The models are pre-trained on NuScenes dataset and fine-tuned on 20% of NuScenes dataset. To fit the scope of the paper, we only use the self-supervised loss when reproducing BEVDistill. Hyperparameters are provided in Appendix A.

Pre-training Method	3D Object Detection		3D Object Tracking		BEV Segmentation	Occupancy Prediction	
	mAP \uparrow	NDS \uparrow	AMOTA \uparrow	AMOTP \downarrow	mIoU \uparrow	mIoU \uparrow	IoU \uparrow
Scratch	51.5 \pm 0.8	53.5 \pm 0.5	57.1 \pm 1.1	80.9 \pm 0.9	39.1 \pm 0.3	15.7 \pm 0.4	32.3 \pm 0.6
BEVDistill	54.1 \pm 0.1	57.5 \pm 0.6	60.6 \pm 0.0	76.5 \pm 0.6	39.1 \pm 0.1	15.8 \pm 0.1	32.3 \pm 0.3
Ours	55.5 \pm 0.5	58.8 \pm 0.5	61.8 \pm 0.7	73.2 \pm 1.2	39.3 \pm 0.1	15.9 \pm 0.2	32.5 \pm 0.1

Table 2. Ablation study about the contributions of the losses we use in our pre-training framework. The models are evaluated on 3D object detection and BEV segmentation task.

Loss func.	3D object det.		BEV seg.
	mAP	NDS	mIoU
Full	55.5 \pm 0.5	58.8 \pm 0.5	39.3 \pm 0.1
$-\mathcal{L}_{MAE}$	54.1 \pm 0.9	58.0 \pm 0.8	39.1 \pm 0.3
$-\mathcal{L}_{CL}$	53.0 \pm 0.4	57.2 \pm 0.3	39.2 \pm 0.2

Table 3. Evaluation on 3D object detection task about the robustness of our pre-training framework when the domain shifts. The models are pre-trained on NuScenes dataset and fine-tuned on 20% of Waymo dataset.

Pre-training Method	L1 mAP	L1 mAPH
Scratch	65.9 \pm 1.1	61.9 \pm 0.9
BEVDistill	64.8 \pm 1.1	60.9 \pm 1.1
Ours	66.6 \pm 0.8	62.6 \pm 0.7

baseline methods. To address whether both the losses in our framework contributes to the performance gain, we provide ablation study by removing one of the loss functions. As shown in Table 2, both loss functions contribute to the improvement of models’ performance on downstream tasks.

Results in held-out setting We fine-tune the NuScenes-pre-trained models on the Waymo dataset for 3D object detection task and test their performance. This will show the robustness of different methods against domain shift. Results in table 3 show that our method also effectively enhances model performance in out-of-distribution scenarios and outperforms baseline methods, demonstrating strong generalization capabilities.

RQ1 Summary:

Our proposed pre-training framework can effectively improve models’ performance on various downstream tasks with the contribution of all losses in both in-domain and out-of-domain scenarios.

4.3. Multi dataset pre-training

In this section, we show that the domain gap between datasets would cause suboptimal model performance and then investigate how our multi-dataset training strategy successfully address this issue. To achieve this, we conduct pre-training under the following configurations:

- Single dataset: Pre-training using only NuScenes dataset.
- Multi-dataset w/o prompt: Pre-training on a naive combination of NuScenes, Lyft, and ONCE datasets.
- Multi-dataset w/ prompt: Pre-training with NuScenes, Lyft, and ONCE, utilizing our prompt training strategy.

Main results Based on the results in Table 4, simply mixing the datasets for pre-training do not effectively improve the model’s performance on downstream tasks, and even perform worse on some tasks than using a single dataset. However, using the prompt-based multi-dataset training strategy lead to a significant performance improvement in all downstream tasks, proving it’s effectiveness of mitigating the domain gap between 3D datasets.

Further analysis One problem people may concern is that during the pre-training phase, we set different tunable prompts for various datasets. However, when applying the pre-trained model to downstream tasks, we do not always use data similar to what was used during pre-training. Thus, the impact of different strategies for using prompts during fine-tuning is crucial. Specifically, when we cannot select an appropriate prompt from those obtained during the pre-training process, is our dataset fusion method still effective? To address this issue, we conduct experiments with the following strategies during fine-tuning on NuScenes dataset:

- W/o prompt: Pre-training with combined dataset without prompt training strategy and then fine-tune.

Table 4. Evaluation on downstream tasks with different pre-training strategies conducted. NuScenes only represents the model is pre-trained using only NuScenes dataset. The others are pre-trained on the fusion dataset combined with NuScenes, Lyft and ONCE with or without dataset prompt. The evaluation is conducted on NuScenes dataset. Hyperparameters are provided in Appendix A.

Pre-training Method	3D Object Detection		3D Object Tracking		BEV Seg.	Occupancy Prediction	
	mAP \uparrow	NDS \uparrow	AMOTA \uparrow	AMOTP \downarrow	mIoU \uparrow	mIoU \uparrow	IoU \uparrow
Single dataset	53.3 ± 0.4	54.2 ± 2.0	58.7 ± 0.4	77.2 ± 1.5	38.9 ± 0.1	16.0 ± 0.4	32.4 ± 0.3
Multi-dataset w/o prompt	52.4 ± 0.9	54.5 ± 0.6	58.0 ± 1.5	78.3 ± 1.1	39.6 ± 0.4	15.9 ± 0.1	31.8 ± 0.2
Multi-dataset w/ prompt	53.6 ± 0.4	56.0 ± 0.5	59.1 ± 0.5	78.2 ± 1.2	41.4 ± 0.1	16.1 ± 0.2	32.5 ± 0.1

Table 5. Comparison of different strategies of using prompt during fine-tuning. The evaluations are conducted using NuScenes dataset on 3D object detection and BEV segmentation task.

Prompt strategie	3D object det.		BEV seg.
	mAP	NDS	mIoU
W/o prompt	52.4 ± 0.9	54.5 ± 0.6	39.6 ± 0.4
Correspond	53.6 ± 0.4	56.0 ± 0.5	41.4 ± 0.1
Wrong	53.1 ± 0.2	55.2 ± 0.6	41.2 ± 0.1

- Correspond: Initialize the prompt of NuScenes with the correct one obtained from pre-training before fine-tuning.
- Wrong: Initialize the prompt of NuScenes with the prompt of another dataset(i.e., ONCE) obtained from pre-training before fine-tuning.

Results in table 5 indicates that even using a mismatched prompt to initialize the model still outperforms a naive dataset mixture. This suggests that our method effectively mitigates conflicts between datasets within the backbone network, preserving generalizable knowledge across datasets.

To further investigate the impact of prompts, we evaluate the models on a sample from the Lyft dataset, applying various prompts or using the model without prompt training, and visualize the BEV heatmap from the image modality. As shown in Figure 3, the prompts enable the model to focus on different angles in space that correspond to the positions of cameras in the dataset. With the correct prompt (i.e., Lyft), the model accurately centers its attention on each camera’s focal area. When there is a mismatch between the data and prompt, the features appear slightly disordered, but can still concentrate on meaningful areas. In contrast, without prompt training strategy, the model struggles to find meaningful feature angles due to conflicts between datasets. Thus, the prompt training strategy effectively mitigates the dataset gap arising from camera angle variations. We provide more experimental results and further analysis in Appendix D.

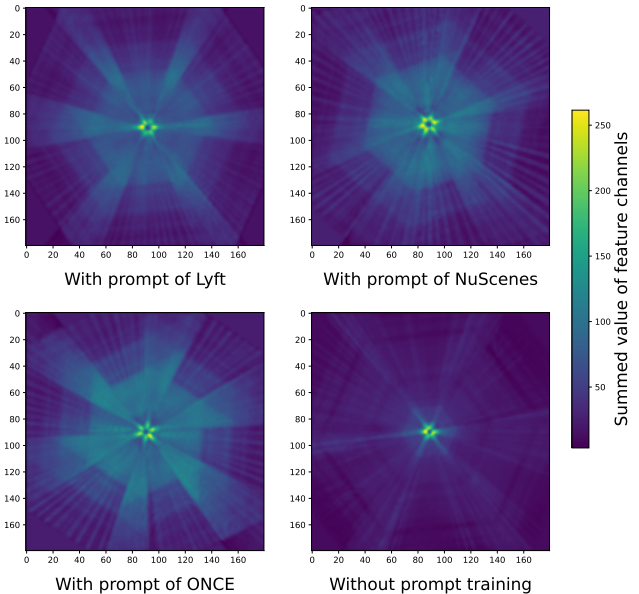


Figure 3. BEV heatmaps of image modality when testing the models by applying various prompts or using the model without prompt training. The x-axis represents the forward and backward direction of the vehicle. The data frame is from Lyft dataset.

RQ2 Summary:

The prompt adapter technique we employ can effectively help mitigate the domain gap between 3D datasets in our self-supervised pre-training framework.

4.4. Scalability of the pre-training methods

The last question we would like to talk about is whether our pre-training method can continually benefit models with the scaling up of data volume. We investigate this issue by conducting experiments on several different training data volumes and compare the model performance on downstream tasks. We progressively expanded the training data volume from 40,000 and 100,000 to 250,000. For the largest experiment, we sample 200,000 frames from ONCE and apply

repeated sampling for four times on the NuScenes and Lyft datasets to balance the scale differences between datasets (Details are provided in Appendix A).

Experimental results in table 6 show that as the training data volume increases, model performance improves steadily. The results indicates that our training method is able to continually improve the performance of 3D perception models with massive training data, thus demonstrating strong scalability.

RQ3 Summary:

Our method shows a steady improvement in model performance as the data scale increases, demonstrating strong scalability and showing potential of utilizing massive training data from the combination of heterogeneous datasets.

5. Related works

3D perception tasks 3D perception focuses on analyzing and interpreting 3D data, including tasks such as detection [2, 7, 10, 13, 15, 20, 21, 25, 27, 28, 31, 33, 44, 47–50, 54–56, 58, 60, 62, 64, 66, 74, 75, 78, 80], segmentation [23, 27, 33, 43, 58, 59, 87], tracking [61, 79] and occupancy prediction [22, 24, 63]. Detection involves identifying and localizing objects within a 3D scene, commonly applied in areas like autonomous driving and robotics. Segmentation refers to partitioning a scene into meaningful regions, using semantic segmentation to label each point with a class, or instance segmentation to separate objects of the same class, which is important in fields like medical imaging. Tracking, on the other hand, involves following the movement of objects over time, crucial in dynamic environments like surveillance and autonomous systems. Occupancy prediction, as a newly proposed task in recent years, involves predicting both voxel occupancy and semantic labels for each voxel, which is essential for generating complete models from partial data and supporting digital twin technology in industrial applications.

Self-supervised pre-training for 3D vision Recently, amounts of works improve the performance of models for 3D Vision tasks via self-supervised pre-training on image and point cloud modalities. For unimodal methods, Contrastive learning [6] and MAE [17] are the most commonly used methods. Contrastive learning methods, which generate similar sample pairs to encourage similar samples to have closer feature representations, are proven to be effective in image modalities [6, 8, 16, 18, 38]. But for point cloud modality, [30, 69, 84] are typically limited to object-level point clouds or smaller indoor scenes due to significant training challenges caused by large scale point clouds. On

the other hand, MAE methods, which train the network to recover masked regions, helping the network capture feature information. Similar to works on the image modality [17, 65, 71], some works [68] directly applying MAE to voxels, but other works [76, 82] modifies the network architecture for better information extraction. For multi-modal methods, many works have used these two modalities in collaboration for pre-training. [26] used super-pixels as a unified encoding view, while [9, 29, 51] used BEV (Bird’s Eye View), and [83] combined both views for training. [36] employed spatial grids as the view for comparing the two modalities. These works often focus on knowledge distillation from one modality to the other. However, [85] found that bidirectional collaborative distillation between the two modalities achieves the best results.

Multi-dataset training for vision tasks Combining multiple datasets for training is an effective method to scale up the amount of training data. However, naively merging different datasets can be harmful for model performance. Relevant studies have been proposed in both the 2D vision field and the point cloud 3D perception field. Researchers have used different normalization layers to differentiate between datasets [59] or have performed category alignment [23, 86] to mitigate the impact of dataset gap. Recent studies [67] have employed prompt techniques to further alleviate the negative impact caused by domain gaps between point clouds from different 3D datasets.

6. Conclusion and discussion

We propose a self-supervised pre-training framework with combined datasets for 3D perception in autonomous driving. Experimental results demonstrate the effectiveness of our methods in utilizing unlabeled data and mitigating the gap between datasets. The scaling experiments shows steady improvement on model performance as the training data volume increases, demonstrating strong scalability and the potential of enabling models to continually evolve toward foundation models with massive training data.

Due to limitations in public datasets and training resources, the scale of datasets and models in our research remains constrained. Our method offers insights for research institutions with access to extensive data and computational resources. For future works, we aim to further exploring the scaling effect of model size for 3D perception models. Additionally, we encourage research institutions to contribute more public datasets, so that the community can collaboratively build foundation models for the 3D perception field with our inspiration.

Table 6. Evaluation of models’ performance on downstream tasks with different scale of pre-training datasets. All experiments are conducted using NuScenes, Lyft and ONCE datasets. Sampling ratios are provided in Appendix A.

Data Volume	3D Object Detection		3D Object Tracking		BEV Segmentation	Occupancy Prediction	
	mAP \uparrow	NDS \uparrow	AMOTA \uparrow	AMOTP \downarrow	mIoU \uparrow	mIoU \uparrow	IoU \uparrow
40K Frame	53.6 \pm 0.7	55.8 \pm 1.8	59.0 \pm 0.2	77.1 \pm 0.4	38.9 \pm 0.2	15.9 \pm 0.2	32.3 \pm 0.4
100K Frame	53.6 \pm 0.4	56.0 \pm 0.5	59.1 \pm 0.5	78.2 \pm 1.2	41.4 \pm 0.1	16.1 \pm 0.2	32.5 \pm 0.1
250K Frame	54.1 \pm 0.6	56.1 \pm 0.3	59.5 \pm 0.7	77.1 \pm 0.7	42.3 \pm 0.3	16.1 \pm 0.1	32.7 \pm 0.1

References

- [1] Jinze Bai, Shuai Bai, Yunfei Chu, Zeyu Cui, Kai Dang, Xiaodong Deng, Yang Fan, Wenbin Ge, Yu Han, Fei Huang, et al. Qwen technical report. [arXiv preprint arXiv:2309.16609](https://arxiv.org/abs/2309.16609), 2023. 1
- [2] Xuyang Bai, Zeyu Hu, Xinge Zhu, Qingqiu Huang, Yilun Chen, Hongbo Fu, and Chiew-Lan Tai. Transfusion: Robust lidar-camera fusion for 3d object detection with transformers. In [Proceedings of the IEEE/CVF conference on computer vision and pattern recognition](https://doi.org/10.1109/CVPR4617.2022.01090), pages 1090–1099, 2022. 8
- [3] Holger Caesar, Varun Bankiti, Alex H Lang, Sourabh Vora, Venice Erin Liong, Qiang Xu, Anush Krishnan, Yu Pan, Giancarlo Baldan, and Oscar Beijbom. nuscenes: A multi-modal dataset for autonomous driving. In [Proceedings of the IEEE/CVF conference on computer vision and pattern recognition](https://doi.org/10.1109/CVPR4617.2022.01162), pages 11621–11631, 2020. 1, 5
- [4] Holger Caesar, Juraj Kabzan, Kok Seang Tan, Whye Kit Fong, Eric Wolff, Alex Lang, Luke Fletcher, Oscar Beijbom, and Sammy Omari. NuPlan: A closed-loop ml-based planning benchmark for autonomous vehicles, 2022. 1
- [5] Mathilde Caron, Hugo Touvron, Ishan Misra, Hervé Jégou, Julien Mairal, Piotr Bojanowski, and Armand Joulin. Emerging properties in self-supervised vision transformers. In [Proceedings of the IEEE/CVF international conference on computer vision](https://doi.org/10.1109/CVPR4617.2022.01162), pages 9650–9660, 2021. 1
- [6] Ting Chen, Simon Kornblith, Mohammad Norouzi, and Geoffrey Hinton. A simple framework for contrastive learning of visual representations. In [ICML](https://doi.org/10.1109/ICML49975.2020.00088), pages 1597–1607, 2020. 8
- [7] Xiaozhi Chen, Huimin Ma, Ji Wan, Bo Li, and Tian Xia. Multi-view 3d object detection network for autonomous driving. In [Proceedings of the IEEE conference on Computer Vision and Pattern Recognition](https://doi.org/10.1109/CVPR4617.2022.01162), pages 1907–1915, 2017. 8
- [8] Xinlei Chen, Haoqi Fan, Ross Girshick, and Kaiming He. Improved baselines with momentum contrastive learning. [arXiv preprint arXiv:2003.04297](https://arxiv.org/abs/2003.04297), 2020. 8
- [9] Zehui Chen, Zhenyu Li, Shiquan Zhang, Liangji Fang, Qin-hong Jiang, and Feng Zhao. Bevdistill: Cross-modal bev distillation for multi-view 3d object detection. [arXiv preprint arXiv:2211.09386](https://arxiv.org/abs/2211.09386), 2022. 1, 5, 8, 13
- [10] Bowen Cheng, Lu Sheng, Shaoshuai Shi, Ming Yang, and Dong Xu. Back-tracing representative points for voting-based 3d object detection in point clouds. In [Proceedings of the IEEE/CVF conference on computer vision and pattern recognition](https://doi.org/10.1109/CVPR4617.2022.01090), pages 8963–8972, 2021. 8
- [11] Christy, Maggie, Niki Nikatos, Phil Culliton, Vinay Shet, and Vladimir Iglovikov. Lyft 3d object detection for autonomous vehicles. <https://kaggle.com/competitions/3d-object-detection-for-autonomous-vehicles>, 2019. Kaggle. 1, 5
- [12] Mostafa Dehghani, Josip Djolonga, Basil Mustafa, Piotr Padlewski, Jonathan Heek, Justin Gilmer, Andreas Peter Steiner, Mathilde Caron, Robert Geirhos, Ibrahim Alabdulmohsin, et al. Scaling vision transformers to 22 billion parameters. In [International Conference on Machine Learning](https://doi.org/10.1109/ICML49975.2022.01162), pages 7480–7512. PMLR, 2023. 1
- [13] Jiajun Deng, Shaoshuai Shi, Peiwei Li, Wengang Zhou, Yanyong Zhang, and Houqiang Li. Voxel r-cnn: Towards high performance voxel-based 3d object detection. In [Proceedings of the AAAI conference on artificial intelligence](https://doi.org/10.1109/AAAI4617.2022.01162), pages 1201–1209, 2021. 8
- [14] Lue Fan, Ziqi Pang, Tianyuan Zhang, Yu-Xiong Wang, Hang Zhao, Feng Wang, Naiyan Wang, and Zhaoxiang Zhang. Embracing single stride 3d object detector with sparse transformer. In [Proceedings of the IEEE/CVF conference on computer vision and pattern recognition](https://doi.org/10.1109/CVPR4617.2022.01090), pages 8458–8468, 2022. 4
- [15] Yulu Gao, Chonghao Sima, Shaoshuai Shi, Shangzhe Di, Si Liu, and Hongyang Li. Sparse dense fusion for 3d object detection. In [2023 IEEE/RSJ International Conference on Intelligent Robots and Systems \(IROS\)](https://doi.org/10.1109/IROS4617.2022.01162), pages 10939–10946. IEEE, 2023. 8
- [16] Kaiming He, Haoqi Fan, Yuxin Wu, Saining Xie, and Ross Girshick. Momentum contrast for unsupervised visual representation learning. In [CVPR](https://doi.org/10.1109/CVPR4617.2022.01162), pages 9726–9735, 2020. 1, 2, 8
- [17] Kaiming He, Xinlei Chen, Saining Xie, Yanghao Li, Piotr Dollár, and Ross Girshick. Masked autoencoders are scalable vision learners, 2021. 1, 2, 8
- [18] Olivier Henaff. Data-efficient image recognition with contrastive predictive coding. In [ICML](https://doi.org/10.1109/ICML49975.2020.00088), pages 4182–4192, 2020. 8
- [19] Georg Hess, Johan Jaxing, Elias Svensson, David Hagerman, Christoffer Petersson, and Lennart Svensson. Masked autoencoder for self-supervised pre-training on lidar point clouds. In [Proceedings of the IEEE/CVF winter conference on applications of computer vision](https://doi.org/10.1109/CVPR4617.2022.01162), pages 350–359, 2023. 1
- [20] Junjie Huang, Guan Huang, Zheng Zhu, Yun Ye, and Dalong Du. Bevdet: High-performance multi-camera 3d object detection in bird-eye-view. [arXiv preprint arXiv:2112.11790](https://arxiv.org/abs/2112.11790), 2021. 8

- [21] Tengting Huang, Zhe Liu, Xiwu Chen, and Xiang Bai. E-pnet: Enhancing point features with image semantics for 3d object detection. In Computer Vision–ECCV 2020: 16th European Conference, Glasgow, UK, August 23–28, 2020, Proceedings, Part XV 16, pages 35–52. Springer, 2020. 8
- [22] Yuanhui Huang, Wenzhao Zheng, Yunpeng Zhang, Jie Zhou, and Jiwen Lu. Tri-perspective view for vision-based 3d semantic occupancy prediction. In Proceedings of the IEEE/CVF conference on computer vision and pattern recognition, pages 9223–9232, 2023. 8
- [23] Dongwan Kim, Yi-Hsuan Tsai, Yumin Suh, Masoud Faraki, Sparsh Garg, Manmohan Chandraker, and Bohyung Han. Learning semantic segmentation from multiple datasets with label shifts. In European Conference on Computer Vision, pages 20–36. Springer, 2022. 8
- [24] Heng Li, Yuenan Hou, Xiaohan Xing, Xiao Sun, and Yanyong Zhang. Occmamba: Semantic occupancy prediction with state space models. arXiv preprint arXiv:2408.09859, 2024. 8, 14
- [25] Yingwei Li, Adams Wei Yu, Tianjian Meng, Ben Caine, Jiquan Ngiam, Daiyi Peng, Junyang Shen, Yifeng Lu, Denny Zhou, Quoc V Le, et al. Deepfusion: Lidar-camera deep fusion for multi-modal 3d object detection. In Proceedings of the IEEE/CVF conference on computer vision and pattern recognition, pages 17182–17191, 2022. 8
- [26] Zhenyu Li, Zehui Chen, Ang Li, Liangji Fang, Qinhong Jiang, Xianming Liu, Junjun Jiang, Bolei Zhou, and Hang Zhao. Simipu: Simple 2d image and 3d point cloud unsupervised pre-training for spatial-aware visual representations. In Proceedings of the AAAI Conference on Artificial Intelligence, pages 1500–1508, 2022. 1, 8, 13
- [27] Zhiqi Li, Wenhui Wang, Hongyang Li, Enze Xie, Chonghao Sima, Tong Lu, Yu Qiao, and Jifeng Dai. Bevfusion: Learning bird’s-eye-view representation from multi-camera images via spatiotemporal transformers. In European conference on computer vision, pages 1–18. Springer, 2022. 4, 8
- [28] Tingting Liang, Hongwei Xie, Kaicheng Yu, Zhongyu Xia, Zhiwei Lin, Yongtao Wang, Tao Tang, Bing Wang, and Zhi Tang. Bevfusion: A simple and robust lidar-camera fusion framework. Advances in Neural Information Processing Systems, 35:10421–10434, 2022. 5, 8
- [29] Jihao Liu, Tai Wang, Boxiao Liu, Qihang Zhang, Yu Liu, and Hongsheng Li. Geomim: Towards better 3d knowledge transfer via masked image modeling for multi-view 3d understanding. In Proceedings of the IEEE/CVF International Conference on Computer Vision, pages 17839–17849, 2023. 1, 8, 13
- [30] Yunze Liu, Li Yi, Shanghang Zhang, Qingnan Fan, Thomas Funkhouser, and Hao Dong. P4contrast: Contrastive learning with pairs of point-pixel pairs for rgb-d scene understanding. arXiv preprint arXiv:2012.13089, 2020. 8
- [31] Yingfei Liu, Tiancai Wang, Xiangyu Zhang, and Jian Sun. Petr: Position embedding transformation for multi-view 3d object detection. In European Conference on Computer Vision, pages 531–548. Springer, 2022. 8
- [32] Ze Liu, Yutong Lin, Yue Cao, Han Hu, Yixuan Wei, Zheng Zhang, Stephen Lin, and Baining Guo. Swin transformer: Hierarchical vision transformer using shifted windows, 2021. 4
- [33] Zhijian Liu, Haotian Tang, Alexander Amini, Xinyu Yang, Huizi Mao, Daniela L Rus, and Song Han. Bevfusion: Multi-task multi-sensor fusion with unified bird’s-eye view representation. In 2023 IEEE international conference on robotics and automation (ICRA), pages 2774–2781. IEEE, 2023. 1, 4, 8
- [34] Jiageng Mao, Minzhe Niu, Chenhan Jiang, Hanxue Liang, Jingheng Chen, Xiaodan Liang, Yamin Li, Chaoqiang Ye, Wei Zhang, Zhenguo Li, et al. One million scenes for autonomous driving: Once dataset. arXiv preprint arXiv:2106.11037, 2021. 1, 5
- [35] Jiageng Mao, Yujing Xue, Minzhe Niu, Haoyue Bai, Jiaoshi Feng, Xiaodan Liang, Hang Xu, and Chunjing Xu. Voxel transformer for 3d object detection. In Proceedings of the IEEE/CVF international conference on computer vision, pages 3164–3173, 2021. 4
- [36] Chen Min, Liang Xiao, Dawei Zhao, Yiming Nie, and Bin Dai. Multi-camera unified pre-training via 3d scene reconstruction. IEEE Robotics and Automation Letters, 2024. 8
- [37] Chen Min, Liang Xiao, Dawei Zhao, Yiming Nie, and Bin Dai. Uniscene: Multi-camera unified pre-training via 3d scene reconstruction for autonomous driving, 2024. 13
- [38] Ishan Misra and Laurens van der Maaten. Self-supervised learning of pretext-invariant representations. In CVPR, pages 6707–6717, 2020. 8
- [39] Yatian Pang, Wenxiao Wang, Francis EH Tay, Wei Liu, Yonghong Tian, and Li Yuan. Masked autoencoders for point cloud self-supervised learning. In European conference on computer vision, pages 604–621. Springer, 2022. 1
- [40] Ziqi Pang, Zhichao Li, and Naiyan Wang. Simpletrack: Understanding and rethinking 3d multi-object tracking. In European Conference on Computer Vision, pages 680–696. Springer, 2022. 14
- [41] Ziqi Pang, Jie Li, Pavel Tokmakov, Dian Chen, Sergey Zagoruyko, and Yu-Xiong Wang. Standing between past and future: Spatio-temporal modeling for multi-camera 3d multi-object tracking. In Proceedings of the IEEE/CVF conference on computer vision and pattern recognition, pages 17928–17938, 2023. 14
- [42] Namuk Park, Wonjae Kim, Byeongho Heo, Taekyung Kim, and Sangdoon Yun. What do self-supervised vision transformers learn? arXiv preprint arXiv:2305.00729, 2023. 3
- [43] Jonah Philion and Sanja Fidler. Lift, splat, shoot: Encoding images from arbitrary camera rigs by implicitly unprojecting to 3d. In Computer Vision–ECCV 2020: 16th European Conference, Glasgow, UK, August 23–28, 2020, Proceedings, Part XIV 16, pages 194–210. Springer, 2020. 8
- [44] Charles R Qi, Or Litany, Kaiming He, and Leonidas J Guibas. Deep hough voting for 3d object detection in point clouds. In proceedings of the IEEE/CVF International Conference on Computer Vision, pages 9277–9286, 2019. 8
- [45] Alec Radford, Jong Wook Kim, Chris Hallacy, Aditya Ramesh, Gabriel Goh, Sandhini Agarwal, Girish Sastry, Amanda Askell, Pamela Mishkin, Jack Clark, Gretchen Krueger, and Ilya Sutskever. Learning transferable visual models from natural language supervision, 2021. 1, 2

- [46] Corentin Sautier, Gilles Puy, Spyros Gidaris, Alexandre Boulch, Andrei Bursuc, and Renaud Marlet. Image-to-lidar self-supervised distillation for autonomous driving data, 2022. 1
- [47] Shaoshuai Shi, Xiaogang Wang, and Hongsheng Li. Pointcnn: 3d object proposal generation and detection from point cloud. In *Proceedings of the IEEE/CVF conference on computer vision and pattern recognition*, pages 770–779, 2019. 8
- [48] Shaoshuai Shi, Chaoxu Guo, Li Jiang, Zhe Wang, Jianping Shi, Xiaogang Wang, and Hongsheng Li. Pv-rcnn: Point-voxel feature set abstraction for 3d object detection. In *Proceedings of the IEEE/CVF conference on computer vision and pattern recognition*, pages 10529–10538, 2020.
- [49] Shaoshuai Shi, Zhe Wang, Jianping Shi, Xiaogang Wang, and Hongsheng Li. From points to parts: 3d object detection from point cloud with part-aware and part-aggregation network. *IEEE transactions on pattern analysis and machine intelligence*, 43(8):2647–2664, 2020.
- [50] Vishwanath A Sindagi, Yin Zhou, and Oncel Tuzel. Mvxnet: Multimodal voxelnet for 3d object detection. In *2019 International Conference on Robotics and Automation (ICRA)*, pages 7276–7282. IEEE, 2019. 8
- [51] Jiachen Sun, Haizhong Zheng, Qingzhao Zhang, Atul Prakash, Z Morley Mao, and Chaowei Xiao. Calico: Self-supervised camera-lidar contrastive pre-training for bev perception. *arXiv preprint arXiv:2306.00349*, 2023. 1, 2, 5, 8, 13
- [52] Pei Sun, Henrik Kretzschmar, Xerxes Dotiwalla, Aurelien Chouard, Vijaysai Patnaik, Paul Tsui, James Guo, Yin Zhou, Yuning Chai, Benjamin Caine, et al. Scalability in perception for autonomous driving: Waymo open dataset. In *Proceedings of the IEEE/CVF conference on computer vision and pattern recognition*, pages 2446–2454, 2020. 1, 5
- [53] Hugo Touvron, Thibaut Lavril, Gautier Izacard, Xavier Martinet, Marie-Anne Lachaux, Timothée Lacroix, Baptiste Rozière, Naman Goyal, Eric Hambro, Faisal Azhar, et al. Llama: Open and efficient foundation language models. *arXiv preprint arXiv:2302.13971*, 2023. 1
- [54] Sourabh Vora, Alex H Lang, Bassam Helou, and Oscar Beijbom. Pointpainting: Sequential fusion for 3d object detection. In *Proceedings of the IEEE/CVF conference on computer vision and pattern recognition*, pages 4604–4612, 2020. 8
- [55] Chunwei Wang, Chao Ma, Ming Zhu, and Xiaokang Yang. Pointaugmenting: Cross-modal augmentation for 3d object detection. In *Proceedings of the IEEE/CVF conference on computer vision and pattern recognition*, pages 11794–11803, 2021.
- [56] Haiyang Wang, Shaoshuai Shi, Ze Yang, Rongyao Fang, Qi Qian, Hongsheng Li, Bernt Schiele, and Liwei Wang. Rbgnnet: Ray-based grouping for 3d object detection. In *Proceedings of the IEEE/CVF Conference on Computer Vision and Pattern Recognition*, pages 1110–1119, 2022. 8
- [57] Haiyang Wang, Chen Shi, Shaoshuai Shi, Meng Lei, Sen Wang, Di He, Bernt Schiele, and Liwei Wang. Dsvt: Dynamic sparse voxel transformer with rotated sets, 2023. 4
- [58] Haiyang Wang, Hao Tang, Shaoshuai Shi, Aoxue Li, Zhen-guo Li, Bernt Schiele, and Liwei Wang. Unitr: A unified and efficient multi-modal transformer for bird’s-eye-view representation. In *Proceedings of the IEEE/CVF International Conference on Computer Vision*, pages 6792–6802, 2023. 1, 5, 8
- [59] Li Wang, Dong Li, Han Liu, Jinzhang Peng, Lu Tian, and Yi Shan. Cross-dataset collaborative learning for semantic segmentation in autonomous driving. In *Proceedings of the AAAI Conference on Artificial Intelligence*, pages 2487–2494, 2022. 8
- [60] Luequan Wang, Hongbin Xu, and Wenxiong Kang. Mv-contrast: Unsupervised pretraining for multi-view 3d object recognition. *Machine Intelligence Research*, 20(6):872–883, 2023. 8
- [61] Qianqian Wang, Yen-Yu Chang, Ruojin Cai, Zhengqi Li, Bharath Hariharan, Aleksander Holynski, and Noah Snavely. Tracking everything everywhere all at once. In *Proceedings of the IEEE/CVF International Conference on Computer Vision*, pages 19795–19806, 2023. 8
- [62] Tai Wang, Xinge Zhu, Jiangmiao Pang, and Dahua Lin. Fcos3d: Fully convolutional one-stage monocular 3d object detection. In *Proceedings of the IEEE/CVF International Conference on Computer Vision*, pages 913–922, 2021. 8
- [63] Xiaofeng Wang, Zheng Zhu, Wenbo Xu, Yunpeng Zhang, Yi Wei, Xu Chi, Yun Ye, Dalong Du, Jiwen Lu, and Xingang Wang. Openoccupancy: A large scale benchmark for surrounding semantic occupancy perception. In *Proceedings of the IEEE/CVF International Conference on Computer Vision*, pages 17850–17859, 2023. 8, 14
- [64] Yue Wang, Vitor Campagnolo Guizilini, Tianyuan Zhang, Yilun Wang, Hang Zhao, and Justin Solomon. Detr3d: 3d object detection from multi-view images via 3d-to-2d queries. In *Conference on Robot Learning*, pages 180–191. PMLR, 2022. 8
- [65] Chen Wei, Haoqi Fan, Saining Xie, Chao-Yuan Wu, Alan Yuille, and Christoph Feichtenhofer. Masked feature prediction for self-supervised visual pre-training. In *Proceedings of the IEEE/CVF Conference on Computer Vision and Pattern Recognition*, pages 14668–14678, 2022. 1, 8
- [66] Hai Wu, Chenglu Wen, Shaoshuai Shi, Xin Li, and Cheng Wang. Virtual sparse convolution for multimodal 3d object detection. In *Proceedings of the IEEE/CVF Conference on Computer Vision and Pattern Recognition*, pages 21653–21662, 2023. 8
- [67] Xiaoyang Wu, Zhuotao Tian, Xin Wen, Bohao Peng, Xi-hui Liu, Kaicheng Yu, and Hengshuang Zhao. Towards large-scale 3d representation learning with multi-dataset point prompt training. In *Proceedings of the IEEE/CVF Conference on Computer Vision and Pattern Recognition*, pages 19551–19562, 2024. 1, 2, 3, 8
- [68] Enze Xie, Zhiding Yu, Daquan Zhou, Jonah Philion, Anima Anandkumar, Sanja Fidler, Ping Luo, and Jose M Alvarez. M2 bev: Multi-camera joint 3d detection and segmentation with unified birds-eye view representation. *arXiv preprint arXiv:2204.05088*, 2022. 8
- [69] Saining Xie, Jiatao Gu, Demi Guo, Charles R Qi, Leonidas Guibas, and Or Litany. Pointcontrast: Unsupervised pre-

- training for 3d point cloud understanding. In Computer Vision–ECCV 2020: 16th European Conference, Glasgow, UK, August 23–28, 2020, Proceedings, Part III 16, pages 574–591. Springer, 2020. 8
- [70] Saining Xie, Jiatao Gu, Demi Guo, Charles R. Qi, Leonidas J. Guibas, and Or Litany. PointContrast: Unsupervised pre-training for 3D point cloud understanding. In ECCV, pages 574–591, 2020. 1, 2
- [71] Zhenda Xie, Zheng Zhang, Yue Cao, Yutong Lin, Jianmin Bao, Zhuliang Yao, Qi Dai, and Han Hu. Simmim: A simple framework for masked image modeling. In Proceedings of the IEEE/CVF conference on computer vision and pattern recognition, pages 9653–9663, 2022. 1, 8
- [72] Junjie Yan, Yingfei Liu, Jianjian Sun, Fan Jia, Shuailin Li, Tiancai Wang, and Xiangyu Zhang. Cross modal transformer: Towards fast and robust 3d object detection. In Proceedings of the IEEE/CVF International Conference on Computer Vision (ICCV), pages 18268–18278, 2023. 1
- [73] Xiangchao Yan, Runjian Chen, Bo Zhang, Jiakang Yuan, Xinyu Cai, Botian Shi, Wenqi Shao, Junchi Yan, Ping Luo, and Yu Qiao. Spot: Scalable 3d pre-training via occupancy prediction for autonomous driving. arXiv preprint arXiv:2309.10527, 2023. 5
- [74] Yan Yan, Yuxing Mao, and Bo Li. Second: Sparsely embedded convolutional detection. Sensors, 18(10):3337, 2018. 8
- [75] Hao Yang, Chen Shi, Yihong Chen, and Liwei Wang. Boosting 3d object detection via object-focused image fusion. arXiv preprint arXiv:2207.10589, 2022. 8
- [76] Honghui Yang, Tong He, Jiaheng Liu, Hua Chen, Boxi Wu, Binbin Lin, Xiaofei He, and Wanli Ouyang. Gd-mae: Generative decoder for mae pre-training on lidar point clouds, 2023. 8
- [77] Hao Yang, Haiyang Wang, Di Dai, and Liwei Wang. Pred: pre-training via semantic rendering on lidar point clouds. Advances in Neural Information Processing Systems, 36, 2024. 5
- [78] Zetong Yang, Yanan Sun, Shu Liu, and Jiaya Jia. 3dssd: Point-based 3d single stage object detector. In Proceedings of the IEEE/CVF conference on computer vision and pattern recognition, pages 11040–11048, 2020. 8
- [79] Tianwei Yin, Xingyi Zhou, and Philipp Krahenbuhl. Center-based 3d object detection and tracking. In Proceedings of the IEEE/CVF conference on computer vision and pattern recognition, pages 11784–11793, 2021. 8
- [80] Jin Hyeok Yoo, Yecheol Kim, Jisong Kim, and Jun Won Choi. 3d-cvf: Generating joint camera and lidar features using cross-view spatial feature fusion for 3d object detection. In Computer vision–ECCV 2020: 16th European conference, Glasgow, UK, August 23–28, 2020, proceedings, part XXVII 16, pages 720–736. Springer, 2020. 8
- [81] Hongcheng Zhang, Liu Liang, Pengxin Zeng, Xiao Song, and Zhe Wang. Sparselif: High-performance sparse lidar-camera fusion for 3d object detection. arXiv preprint arXiv:2403.07284, 2024. 1
- [82] Renrui Zhang, Ziyu Guo, Peng Gao, Rongyao Fang, Bin Zhao, Dong Wang, Yu Qiao, and Hongsheng Li. Point-m2ae: multi-scale masked autoencoders for hierarchical point cloud pre-training. Advances in neural information processing systems, 35:27061–27074, 2022. 1, 8
- [83] Sha Zhang, Jiajun Deng, Lei Bai, Houqiang Li, Wanli Ouyang, and Yanyong Zhang. Hvdistill: Transferring knowledge from images to point clouds via unsupervised hybrid-view distillation. International Journal of Computer Vision, pages 1–15, 2024. 2, 8
- [84] Zaiwei Zhang, Rohit Girdhar, Armand Joulin, and Ishan Misra. Self-supervised pretraining of 3d features on any point-cloud. In Proceedings of the IEEE/CVF International Conference on Computer Vision, pages 10252–10263, 2021. 8
- [85] Shengchao Zhou, Weizhou Liu, Chen Hu, Shuchang Zhou, and Chao Ma. Unidistill: A universal cross-modality knowledge distillation framework for 3d object detection in bird’s-eye view, 2023. 1, 8, 13
- [86] Xingyi Zhou, Vladlen Koltun, and Philipp Krähenbühl. Simple multi-dataset detection. In Proceedings of the IEEE/CVF conference on computer vision and pattern recognition, pages 7571–7580, 2022. 8
- [87] Xinge Zhu, Hui Zhou, Tai Wang, Fangzhou Hong, Yuexin Ma, Wei Li, Hongsheng Li, and Dahua Lin. Cylindrical and asymmetrical 3d convolution networks for lidar segmentation. In Proceedings of the IEEE/CVF conference on computer vision and pattern recognition, pages 9939–9948, 2021. 8

A. Hyperparameters & configurations of pre-training

For experiments in Table 1 in section 4.2, we use a linear lr warm up and then use a cosine lr decay policy to reduce the lr to 0.01 times of the peak value. We conducted parameter search for learning rate and the final parameters are as in table 7.

Parameter	Value
Learning rate	4e-4
Batch size	32
Training epochs	50
LR warm epoches	5
Weight decay	0.01

Table 7. Hyperparameters of pre-training in table 1

For experiments in Table 4, 5 and 6, we keep the settings except for setting learning rate to 2e-4. The dataset volume and repeat sampling times in each epoch for experiments in Table 6 are provided in Table 8.

B. Discussion on baselines & related works

In previous research, many pre-training methods for point cloud and image modality collaboration have been proposed. These methods transform images and point clouds into a unified perspective for joint training. Based on the chosen perspective, they can be categorized into three types: superpixel-based, BEV-based, and occupancy-based methods.

Occupancy-based methods such as UniScene [37] construct spatial occupancy grids from point clouds and reconstruct these grids using image modality data. These methods primarily focus on pre-training image networks, offering limited utility in multimodal 3D perception scenarios.

Superpixel-based methods, such as SimIPU [26], divide images into superpixels and treat the corresponding point cloud regions within each superpixel as a single unit for comparison. However, these methods are incompatible with modern BEV-based 3D perception models.

BEV-based methods unify image and point cloud information in the BEV perspective for comparison. The most representative works is BEVDistill [9]. GeoMIM [29] and UniDistill [85] have modified this approach. Their training objectives often involves distilling 3D information from point clouds into the image modality or transferring knowledge from pre-trained image backbones to point cloud backbones. These methods typically use MSE loss to directly align the features of the student modality with those of the teacher modality. However, this setup is not suitable for training models in point cloud-image fusion scenarios from

scratch. Additionally, these works rely on labeled data to train decoders for object-level distillation, which limits their scalability.

The most recent research, CALICO [51], compares superpixel-based and BEV-based methods, highlighting that BEVDistill-type approaches offer better performance and greater potential for improvement. CALICO uses image-point cloud contrastive loss and a point-cloud-only self-contrastive loss, emphasizing the training of point cloud networks. However, CALICO is not open-sourced and relies on relatively traditional backbone networks, making direct comparisons difficult.

Given these reasons, we follow CALICO and adopt the most relevant BEVDistill method as our experimental baseline, modifying it to fit a self-supervised learning framework by removing the object-level distillation loss that depends on labeled data.

C. Details of downstream tasks

C.1. 3D object detection

In this section, we describe the detailed experimental setups used in our downstream tasks. To leverage the advantages of multimodal pretraining, we employed the BEVFusion multimodal framework to perform downstream 3D object detection and BEV map segmentation tasks. For the image and LiDAR backbones, we utilized Swin-Transformer and DSVT, with an image size of [256, 704] and a voxel size of [0.3, 0.3, 8], respectively. The resulting BEV feature maps for LiDAR and Camera are sized [180, 180, 128] and [180, 180, 80], respectively. We concatenated these two BEV feature maps and applied a fusion layer, followed by a BEV backbone and an FPN network. For 3D detection, we used the Transfusion head with 8×3 batches on the NuScenes dataset and the DSVT head with 8×4 batches on the Waymo dataset. For both datasets, we employed the AdamW optimizer with a cyclic scheduler and a starting learning rate of 1×10^{-4} . Additionally, we used ground-truth copy-paste data augmentation during training, which was disabled in the last five epochs.

When we get pre-trained checkpoint, we just load parameters of Swin-Transformer and DSVT backbones. For "Correspond" setting, we fix the prompt to "NuScenes", and "Once" for "Wrong" setting. For "Random" setting, we train the prompt from scratch.

C.2. BEV map segmentation

For BEV map segmentation, we employ the same framework as 3D object detection, but with a different head. We use the same BEVSegmentationHead as BEVFusion, first obtaining 200×200 BEV features through linear interpolation, and then apply a convolutional layer to predict the class of each grid. We employed the AdamW optimizer with a

Experiment	NuScenes		NuScenes		NuScenes	
	Data volume	Repeat times	Data volume	Repeat times	Data volume	Repeat times
40K Frame	13,300	1	13,300	1	13,300	1
100K Frame	28,130	1	22,680	1	50,000	1
250K Frame	28,130	4	22,680	4	200,000	1

Table 8. Configures of dataset sampling for pre-training in table 6.

cyclic scheduler, starting with a learning rate of 1×10^{-4} . The model’s performance was evaluated on the NuScenes dataset. Finally, the handling of the pre-trained checkpoint follows the same approach as in 3D object detection.

C.3. 3D object tracking

In the task of 3D object tracking, we utilize SimpleTrack [40], a ”tracking-by-detection” framework directly leveraging detection results as input. Initially, the input detections are pre-processed to select the ones to be used for tracking. Subsequently, a motion model is employed to predict and update the states of the tracked objects. After generating predictions across frames, a data association step is performed to link detections with existing tracklets. In addition to the core algorithmic steps, ”birth”, ”death” and ”output” policies are implemented to manage the life-cycle of detections and tracklets. For the nuScenes dataset, we adhere to the default hyper-parameter settings in SimpleTrack, which include using 3D GIoU as the association metric and applying a score threshold of 0.01 for output bounding boxes. These settings are well-suited for detectors incorporating LiDAR modalities[41].

C.4. Occupancy prediction

In Occupancy Prediction task, we utilize the OpenOccupancy dataset [63], which is an occupancy annotation dataset derived from the nuScenes dataset and adheres to its data format. The dataset includes 700 training sequences and 150 validation sequences, with annotations provided for 17 different classes. For each input frame, we use six surround-view camera images resized to [256, 704] as visual input and fuse ten frames of LiDAR points covering a spatial range of [-51.2m, 51.2m] along both the X and Y axes and [-2.0m, 6.0m] along the Z axis. The occupancy annotations are mapped onto a voxel grid of dimensions $512 \times 512 \times 40$, with each voxel measuring 0.2 meters. In terms of model architecture, we build upon the OccMamba [24] framework, setting mamba features dimension to 128 and replacing the backbones for the image and LiDAR inputs with Swin-Transformer and DSVT, respectively, as referenced in the aforementioned works. For our training strategy, we increase the learning rate to $5e-4$ based on OccMamba. Specifically, during training with the

dataset prompt, we fix the learnable prompt in PromptNorm to ensure better results on this challenging task. All other model and training configurations remain consistent with the original OccMamba settings.

D. Analysis of prompts

To further investigate the role of prompts in the model, we visualized the image BEV heatmap, as shown in Figure 4 4, where the x-axis represents the forward direction of the vehicle. We extracted one sample each from the NuScenes, ONCE, and Lyft datasets and tested them using networks with different prompts or without prompts. The visualization reveals that the image BEV features tend to cluster in specific regions across all three datasets.

In these datasets, the image data are collected from six camera views: front, front-left, front-right, rear-left, rear-right, and rear. Due to calibration issues, slight tilts may occur, and variations in viewing angles and other camera parameters exist among the datasets. Figure 4 4 highlights that when the correct prompt is applied, the network can effectively focus feature information on the central regions captured by the cameras, thereby extracting more valuable features. In contrast, using incorrect prompts still produces a clustering effect, but the focus is less precise. Without employing the prompt training strategy during training, the feature distribution becomes highly disorganized or the model fails to capture meaningful features.

This visualization underscores the importance of prompts in guiding the model to align features accurately with the input data’s intrinsic structure address the domain gap between datasets.

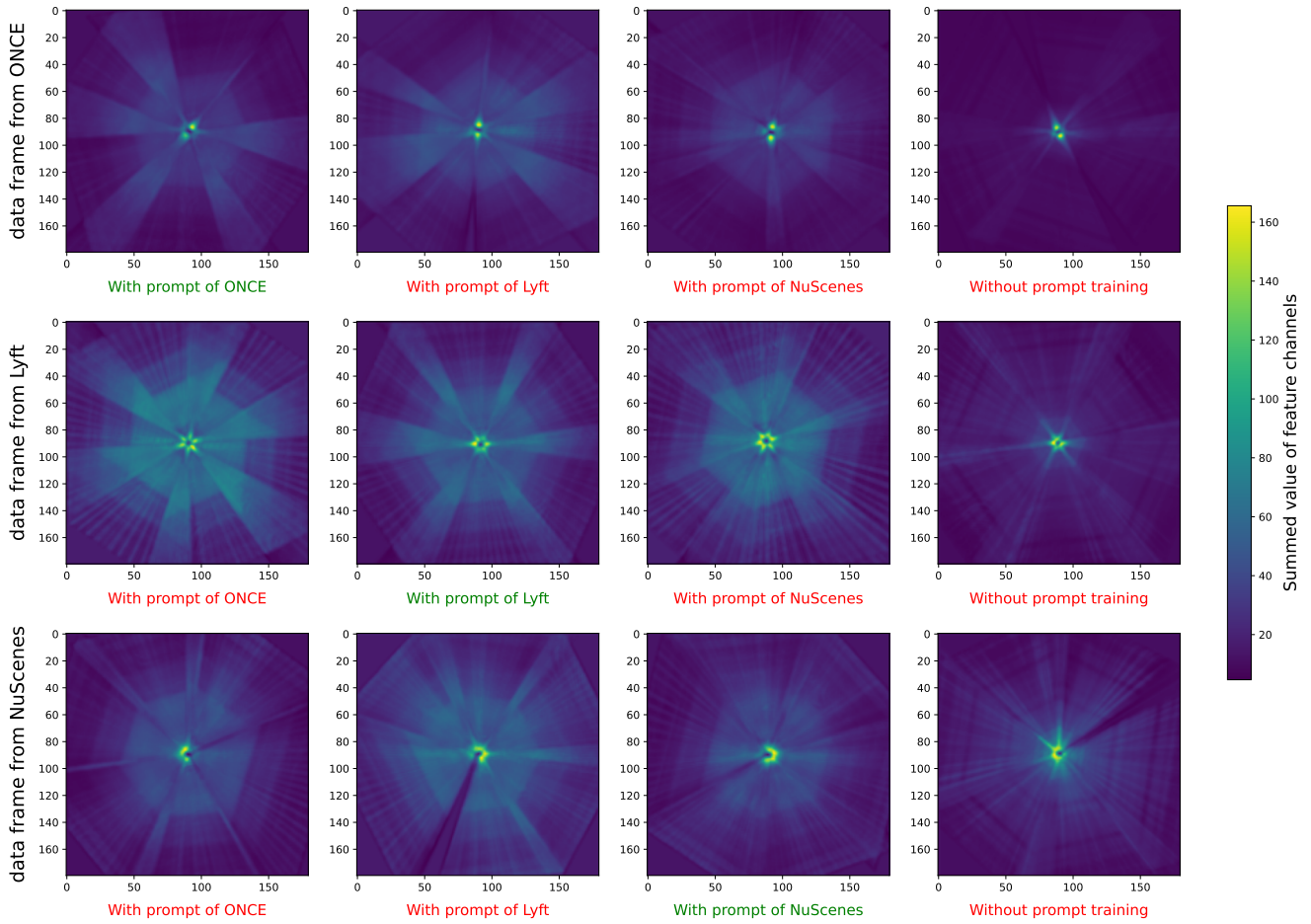


Figure 4. BEV heatmaps of image modality when testing the models by applying various prompts or using the model without prompt training.